HHS Public Access

Author manuscript

J Am Chem Soc. Author manuscript; available in PMC 2021 February 25.

Published in final edited form as:

J Am Chem Soc. 2017 September 13; 139(36): 12406–12409. doi:10.1021/jacs.7b07272.

Cyanine Conformational Restraint in the Far-Red Range

Megan S. Michie[†], **Ralph Götz**[‡], **Christian Franke**[‡], **Matthew Bowler**[§], **Nikita Kumari**[‖], **Valentin Magidson**[⊥], **Marcia Levitus**[‖], **Jadranka Loncarek**[#], **Markus Sauer**[‡], **Martin J. Schnermann**[*,†]

[†]Laboratory of Chemical Biology, NIH/NCI/CCR, 376 Boyles Street, Frederick, Maryland 21702, United States

[‡]Department of Biotechnology and Biophysics, Julius Maximilian University Würzburg, Am Hubland 97074 Würzburg, Germany

[§]Optical Microscopy and Analysis Laboratory, NIH/NCI/CCR, 1050 Boyles Street, Frederick, Maryland 21702, United States

[‖]School of Molecular Sciences and The Biodesign Institute at Arizona State University, Tempe, Arizona 85287, United States

[⊥]Optical Microscopy and Analysis Laboratory, Leidos Biomedical Res. Inc., Frederick National Laboratory for Cancer Research, Frederick, Maryland 21702, United States

[#]Laboratory of Protein Dynamics and Signaling, NIH/NCI/CCR, 1050 Boyles Street, Frederick, Maryland 21702, United States

Abstract

Far-red cyanine fluorophores find extensive use in modern microscopy despite modest quantum yields. To improve the photon output of these molecules, we report a synthetic strategy that blocks the major deactivation pathway: excited-state *trans*-to-*cis* polyene rotation. In the key transformation, a protected dialdehyde precursor undergoes a cascade reaction to install the requisite tetracyclic ring system. The resulting molecules exhibit the characteristic features of conformational restraint, including improved fluorescence quantum yield and extended lifetime. Moreover, these compounds recover from hydride reduction with dramatically improved efficiency. These observations enable efficient single-molecule localization microscopy in oxygenated buffer without addition of thiols. Enabled by modern organic synthesis, these studies provide a new class of far-red dyes with promising spectroscopic and chemical properties.

Single molecule localization microscopy (SMLM) techniques like photoactivated localization microscopy (PALM) and *direct* stochastic optical reconstruction microscopy (*d*STORM) enable three-dimensional (3D) imaging of cellular components with nearly molecular resolution.[1–3] Localization precision, and therefore the structural resolution

[*]**Corresponding Author**: martin.schnermann@nih.gov, Martin J. Schnermann.

Supporting Information

The Supporting Information is available free of charge on the ACS Publications website at DOI: 10.1021/jacs.7b07272.

Synthetic and imaging methods, and supplementary figures (PDF)

The authors declare no competing financial interest.

capability of SMLM, scales with the inverse square root of the single molecule emitter intensity.[4] Consequently, SMLM fluorophores should provide high photon yields in the on state, while exhibiting low to absent background fluorescence in the off state. Small molecules, in combination with various targeting strategies, are often uniquely well-suited to these applications.[5]

Indocyanines are among the most useful fluorescent small molecules, uniquely spanning the visible to near-infrared range through successive 2-carbon homologation.[6–8] Far-red variants, including Cy5 and Alexa 647 (AF647), are the most common chemical component of *d*STORM methods.[9–11] However, fluorescence quantum yields (Φ_F) are modest, typically below 0.2 in aqueous solution.[12] Cyanine excited state deactivation involves *trans*- to *cis*-polyene rotation that competes extensively with photon emission.[12,13] In the trimethine series, which emits in the green region of the spectrum, this pathway has been obstructed through installation of fused 6-membered rings to the polymethine bridge, leading to dramatically improved Φ_F (Figure 1A).[14–16] Extending this approach to the far-red cyanines could provide needed brighter fluorophores in this spectral range, but requires the synthesis of a complex fused tetracyclic ring system (Figure 1B).

Here we describe the first synthetic strategy to assemble conformationally restrained pentamethine indocyanines. The key reaction is a cyclization cascade of a protected dialdehyde precursor, which is accessed through chemoselective olefin metathesis (Figure 1C). The resulting far-red fluorophores exhibit improved fluorescence quantum yields and extended lifetimes relative to unrestrained pentamethine cyanines. In addition, we find these constrained cyanines recover from hydride reduction with superior efficiency relative to existing far-red cyanines. These observations enable SMLM, providing resolution and photon output in oxygenated phosphate-buffered saline (PBS) exceeding that obtained with conventional cyanines in the optimized photoswitching buffers used in *d*STORM.[9,17]

The retrosynthetic analysis is shown in Figure 1C. In the key reaction, a protected dialdehyde undergoes intramolecular Michael addition followed by a dihydropyran ring-forming cascade. The latter sequence, but not the Michael addition, is analogous to that employed in the assembly of the Cy3B scaffold.[14] As the cyanine polyene is incompatible with nucleophilic olefination methods, a critical challenge is the chemoselective introduction of the sensitive *α,β*-unsaturated aldehyde motif (or synthetic equivalent). A cross-metathesis reaction was ultimately found to provide a suitable means to install an unsaturated acetal.[18]

We first targeted the unsubstituted restrained indocyanine **4** (Scheme 1A). Precursor **1** was assembled through the conventional route from *N*-alkylated indolenines (see SI). Cross-metathesis using the Grubbs second-generation catalyst (30 mol %),[18] and acrolein dimethyl acetal (**2**, 10 equiv) in CH_2Cl_2 at 40 °C provided **3** in 62% yield following SiO_2 purification. Compound **3** underwent tetracyclization in a 4:1 mixture of $CHCl_3$:7 N H_2SO_4 at 70 °C to provide **4** as a single diastereomer in 24% yield. This structure, including the *syn–syn* ring junction stereochemistry, was assigned by NMR analysis (Figure S1). In examining alternative cyclization conditions, we found that exposing **3** to BBr_3 in CH_2Cl_2 at −78 °C provided **4** and a second compound, which was obtained in a variable ratio (~1:1 to ~2:1). The inseparable mixture exhibits a single $[M]^+$ ion signal, complex NMR signals in the

dihydropyran region, and a single far-red UV–vis absorbance maximum (Figure S2). Compound **4** and the second compound, tentatively assigned to be a diastereomer, can be equilibrated to homogeneous **4** in 1:3 MeOH:0.3 M HCl at 60 °C with an improved two-step yield from **3** of 53% (Figure 1A). Computational analysis indicates the lowest energy diastereomer containing an *anti*-ring junction is diastereomeric to **4** adjacent to C5′ of the polyene (Figure S3). Of note, simply subjecting **3** to the MeOH:HCl equilibration conditions provided only trace quantities of **4**.

To gain access to a conjugatable variant, we adopted a related strategy starting from cyanine **5** (see SI for synthesis). Cross-metathesis using Hoyveda-Grubbs second-generation catalyst (50 mol %)[19] proceeds efficiently between **5** and **2** at rt to provide **6**, which was used without extensive purification (Scheme 1B). Though the tetracyclization cascade of **6** was incompatible with the biphasic aqueous acidic conditions, the use of BBr_3 in CH_2Cl_2 at −78 °C provided a similar mixture to that obtained with **4** (Figure S4). Equilibration in 1:3 MeOH:0.3 M HCl at 60 °C gave the methyl ester which, after saponification and reverse phase purification, provided **7** in a useful four-step yield of 42%. To prepare bioconjugates, **7** was converted to the carboxylic acid **8** through a straightforward amide coupling sequence. Phalloidin conjugate **9** was then obtained by NHS-ester generation and amide bond formation.

To our delight, compounds **4** and **7** exhibit the characteristic features of conformational restriction. The Φ_F is increased from0.15 (MeOH) with **10** (Figure 2A) to 0.69 (MeOH) and 0.55 (PBS) with **4** and **7**, respectively (Figure 2B). This occurs with a shift in λ_{max} of approximately 25 nm in both cases (Figure 2B,C). Both fluorescence lifetime and Φ_F are largely solvent viscosity insensitive, unlike with the conventional pentamethine cyanine **10** that is subject to photoisomerization (Table S1). Moreover, also unlike with **10**, the emission of **4** is insensitive to temperature (Figure 2D). This is also due to photoisomerization in **10**, which becomes more efficient at higher temperatures. The substantially longer lifetimes of **4** and **7** relative to the unrestrained cyanine **10** point to significant potential for fluorescence lifetime imaging microscopy (FLIM).[20]

Motivated by these auspicious properties, we then investigated if these fluorophores could be applied in SMLM experiments. A central feature of SMLM is the photoactivation or conversion of fluorophores between fluorescent and non-fluorescent states.[21] Three modes of cyanine reactivity have been applied in this context: reversible formation of (1) thioland (2) phosphine-polyene adducts, as well as (3) sequential reduction/oxidation of the imine-like C2-N double bond.[22–25] Noting that the reactivity of existing cyanines in these chemistries varies widely,[11,25] we examined the new molecules. In an unanticipated consequence of conformational restraint, the UV-light induced regeneration of **4** following $NaBH_4$ reduction is dramatically enhanced relative to unrestrained cyanines. Treatment of **4** and **10** with 2.0 equiv of $NaBH_4$ afforded the corresponding reduced product (Figure S5A,B).[26] Strikingly, photolysis of a 20 μM solution in 4:1 PBS:DMSO with UV light (365 nm, 5 mW/cm^2) provides 38% maximal cyanine absorbance recovery with 4 after 5 min, but only a 6% maximal recovery after 30 min with **10** (Figure 2E). Of note, the degree of recovery in these ensemble studies is lower than seen in the microscopy studies below,

which were carried out at much lower concentration. In examining other types of cyanine photoconversion, we found the phosphine adducts observed with conventional pentamethine cyanines, such as AF647, are not observed with **7** (Figure S6). Suggesting that the thiol adducts are also disfavored by ring constraint, SMLM with **9** under typical STORM conditions (high thiol, deoxygenated buffer) did not afford a useful reconstruction (Figure S7).

Phalloidin conjugate **9** was applied to visualize cellular Factin in initial wide-field studies. These efforts included comparisons to the commercially available Alexa Fluor 647-phalloidin conjugate (AF647-phalloidin), which has been used extensively. We observed that reduction and UV-activation of **9** provides dramatically improved recovery relative to AF647-phalloidin (Figure S8). We also found that photostability of 9 was nearly indistinguishable from that of AF647-phalloidin (Figure S9).

We then applied the phalloidin conjugate **9** to 3D PALM-like super-resolution imaging. We utilized a biplane imaging scheme (BP)[27] in combination with TRABI[28] to simultaneously precisely quantify single molecule intensities and perform TRABI-BP imaging. Labeling and reduction (26 mM $NaBH_4$) with subsequent imaging in non-degassed PBS provided high quality 3D super-resolved images of the actin cytoskeleton (Figure 3, Figure S10). In TRABI-BP experiments, we detected on average 5181 photons per frame (median) from single activated dyes, whereas tracking emitters that are active in consecutive frames yielded a conflated photon count of 6961 (median) before photobleaching or conversion to a non-fluorescent form. This corresponds to experimentally measured localization precisions of 5–7 nm laterally and ~20 nm axially. Excitation with either 640 or 660 nm light can be employed, with the latter providing somewhat improved photon yield (Figure S11). We also found that while the UV-laser can accelerate the recovery, the photoactivation rate obtained using solely the excitation laser (either 640 or 660 nm) was sufficient to generate an emitter density suitable for SMLM. Interestingly, in SMLM experiments, recovery of the reduced state proceeds almost quantitatively if 405 nm light is applied only for very short time periods. By contrast, when AF647-phalloidin was subjected to the reduction/recovery sequence, no reconstruction could be obtained. We have compared the images obtained with **9** using the reductive method with AF647 under standard *d*STORM buffer conditions. Conjugate **9** gave similar, if slightly improved, photon counts relative to AF647-phalloidin (**9**: 3721 per frame, 5107 tracked; AF647:3422 per frame, 3737 tracked) and localization precisions of 5.2 and 5.9 nm, respectively (Figure 3).

In summary, we have developed a cascade cyclization strategy that appends a tetracyclic ring system to the pentamethine cyanine polymethine bridge. Conformational restraint improves fluorescence quantum yield and prolongs lifetime, while also enhancing recovery from hydride addition. These properties enable PALM-like SMLM, providing excellent photon counts without recourse to high thiol, deoxygenated buffer. The combination of these new cyanines and reductive caging may be useful in other contexts, including live-cell localization and tracking experiments. Additionally, the improved recovery of the new variants may be enabling for sensing reactive oxygen species (ROS), another context where cyanine reduction/oxidation has been used.[26]

These studies provide the chemical framework to create fluorophores targeting a range of applications. For example, the installation of additional sulfonates or other polar functional groups is likely a prerequisite for antibody labeling at high density.[29] The application of strategies to mitigate photobleaching reactions could extend the time window for observation.[30–33] These and related efforts are the subject of ongoing investigation.

Supplementary Material

Refer to Web version on PubMed Central for supplementary material.

ACKNOWLEDGMENTS

M.J.S. thanks Dr. Joseph Barchi, NCI-CCR, for NMR assistance and Dr. James Kelley, NCI-CCR, for mass spectrometric analysis. This work was supported by the Intramural Research Program of the National Institutes of Health, National Cancer Institute, Center for Cancer Research. M.S. acknowledges funding by the DFG (ReceptorLight TRR 166). Dr. Luke Lavis, Janelia Research Campus, Howard Hughes Medical Institute, is acknowledged for assistance with fluorescence quantum yield determination and helpful discussions.

REFERENCES

(1). Sauer M; Heilemann M Chem. Rev 2017, 117, 7478. [PubMed: 28287710]
(2). Sengupta P; van Engelenburg SB; Lippincott-Schwartz J Chem. Rev 2014, 114, 3189. [PubMed: 24417572]
(3). Huang B; Bates M; Zhuang X Annu. Rev. Biochem 2009, 78, 993. [PubMed: 19489737]
(4). Mortensen KI; Churchman LS; Spudich JA; Flyvbjerg H Nat. Methods 2010, 7, 377. [PubMed: 20364147]
(5). Grimm JB; English BP; Chen JJ; Slaughter JP; Zhang ZJ; Revyakin A; Patel R; Macklin JJ; Normanno D; Singer RH; Lionnet T; Lavis LD Nat. Methods 2015, 12, 244. [PubMed: 25599551]
(6). Mishra A; Behera RK; Behera PK; Mishra BK; Behera GB Chem. Rev 2000, 100, 1973. [PubMed: 11749281]
(7). Gorka AP; Nani RR; Schnermann MJ Org. Biomol. Chem 2015, 13, 7584. [PubMed: 26052876]
(8). Mujumdar RB; Ernst LA; Mujumdar SR; Lewis CJ; Waggoner AS Bioconjugate Chem. 1993, 4, 105.
(9). van de Linde S; Loschberger A; Klein T; Heidbreder M; Wolter S; Heilemann M; Sauer M Nat. Protoc 2011, 6, 991. [PubMed: 21720313]
(10). Heilemann M; van de Linde S; Mukherjee A; Sauer M Angew. Chem., Int. Ed 2009, 48, 6903.
(11). Dempsey GT; Vaughan JC; Chen KH; Bates M; Zhuang X Nat. Methods 2011, 8, 1027. [PubMed: 22056676]
(12). Levitus M; Ranjit SQ Rev. Biophys 2011, 44, 123.
(13). Stennett EMS; Ciuba MA; Levitus M Chem. Soc. Rev 2014, 43, 1057. [PubMed: 24141280]
(14). Waggoner AS; Mujumdar RB Rigidized Trimethine Cyanine Dyes. U.S. Patent 6133445A, 10. 17, 2000.
(15). Cooper M; Ebner A; Briggs M; Burrows M; Gardner N; Richardson R; West RJ Fluoresc. 2004, 14, 145.
(16). Sanborn ME; Connolly BK; Gurunathan K; Levitus MJ Phys. Chem. B 2007, 111, 11064.
(17). Heilemann M; Margeat E; Kasper R; Sauer M; Tinnefeld PJ Am. Chem. Soc 2005, 127, 3801.
(18). Chatterjee AK; Choi TL; Sanders DP; Grubbs RH J. Am. Chem. Soc 2003, 125, 11360. [PubMed: 16220959]
(19). Garber SB; Kingsbury JS; Gray BL; Hoveyda AH J. Am. Chem. Soc 2000, 122, 8168.
(20). Niehorster T; Loschberger A; Gregor I; Kramer B; Rahn HJ; Patting M; Koberling F; Enderlein J; Sauer M Nat. Methods 2016, 13, 257. [PubMed: 26808668]

(21). Chozinski TJ; Gagnon LA; Vaughan JC FEBS Lett. 2014, 588, 3603. [PubMed: 25010263]
(22). Dempsey GT; Bates M; Kowtoniuk WE; Liu DR; Tsien RY; Zhuang XJ Am. Chem. Soc 2009, 131, 18192.
(23). Vaughan JC; Dempsey GT; Sun E; Zhuang XJ Am. Chem. Soc 2013, 135, 1197.
(24). Vaughan JC; Jia S; Zhuang X Nat. Methods 2012, 9, 1181. [PubMed: 23103881]
(25). Lehmann M; Gottschalk B; Puchkov D; Schmieder P; Schwagerus S; Hackenberger CP; Haucke V; Schmoranzer J Angew. Chem., Int. Ed 2015, 54, 13230.
(26). Kundu K; Knight SF; Willett N; Lee S; Taylor WR; Murthy N Angew. Chem., Int. Ed 2009, 48, 299.
(27). Ram S; Prabhat P; Chao J; Ward ES; Ober RJ Biophys. J 2008, 95, 6025. [PubMed: 18835896]
(28). Franke C; Sauer M; van de Linde S Nat. Methods 2017, 14, 41. [PubMed: 27869814]
(29). Initial antibody labeling studies with NHS-esters of 7 and 8 resulted in significant H-aggregate formation.
(30). Altman RB; Terry DS; Zhou Z; Zheng Q; Geggier P; Kolster RA; Zhao Y; Javitch JA; Warren JD; Blanchard SC Nat. Methods 2012, 9, 68.
(31). Renikuntla BR; Rose HC; Eldo J; Waggoner AS; Armitage BA Org. Lett 2004, 6, 909. [PubMed: 15012062]
(32). Toutchkine A; Nguyen DV; Hahn KM Org. Lett 2007, 9, 2775. [PubMed: 17583344]
(33). Gorka AP; Schnermann MJ Curr. Opin. Chem. Biol 2016, 33, 117. [PubMed: 27348157]

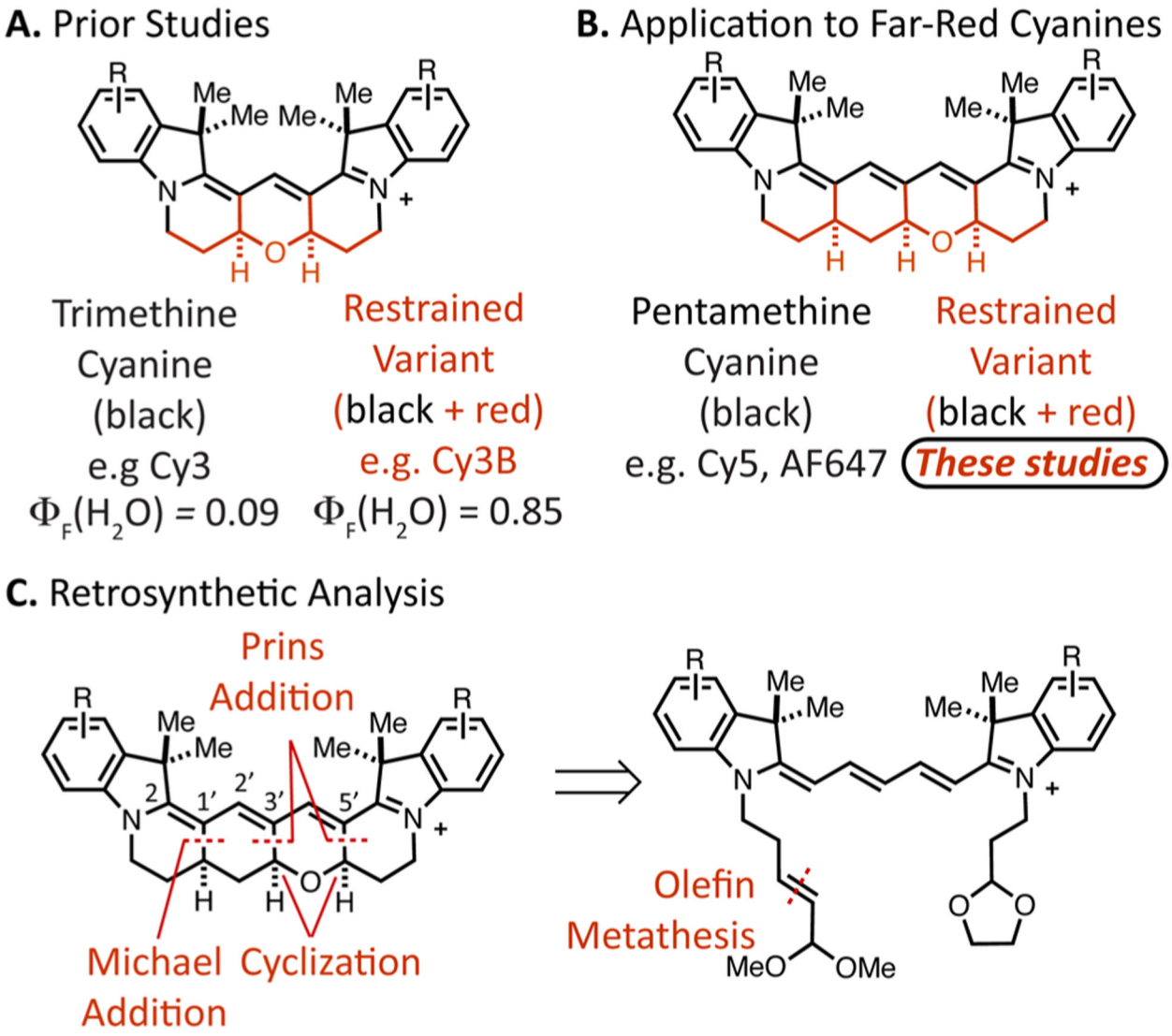

Figure 1.

(A) Conformational restraint applied to trimethine cyanines,(B) application to far-red cyanines (these studies), and (C) retrosynthesis.

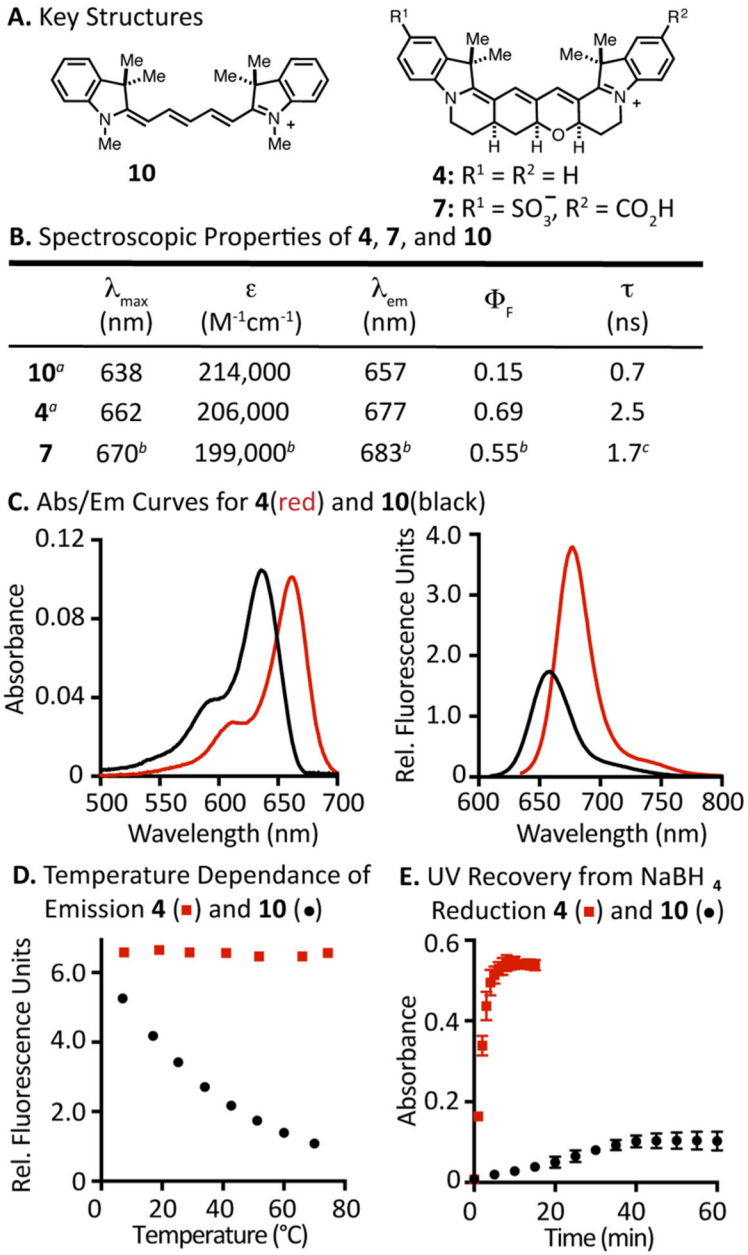

	λ_{max} (nm)	ε ($M^{-1}cm^{-1}$)	λ_{em} (nm)	Φ_F	τ (ns)
10[a]	638	214,000	657	0.15	0.7
4[a]	662	206,000	677	0.69	2.5
7	670[b]	199,000[b]	683[b]	0.55[b]	1.7[c]

Figure 2.

(A) Key structures and (B) their spectroscopic properties. (C) Absorbance/emission curves for **4** and **10** (750 nM in MeOH). (D) Temperature Dependence of the Emission of **4** (red ■) and 10 (black ●) (in EtOH) (E) UV recovery of 20 μM **4** (red ■) and **10** (black ●) (in 4:1 PBS (50 mM, pH 7.4):DMSO) following $NaBH_4$ reduction (2.5 mM in 1:1 DMSO:MeOH). Absorbance at λ_{max} (**4** at 640 nm and **10** at 660 nm) as a function of 365 nm irradiation time (5 mW/cm^2). [a]In MeOH. [b]In pH 7.4 PBS. [c]In H_2O.

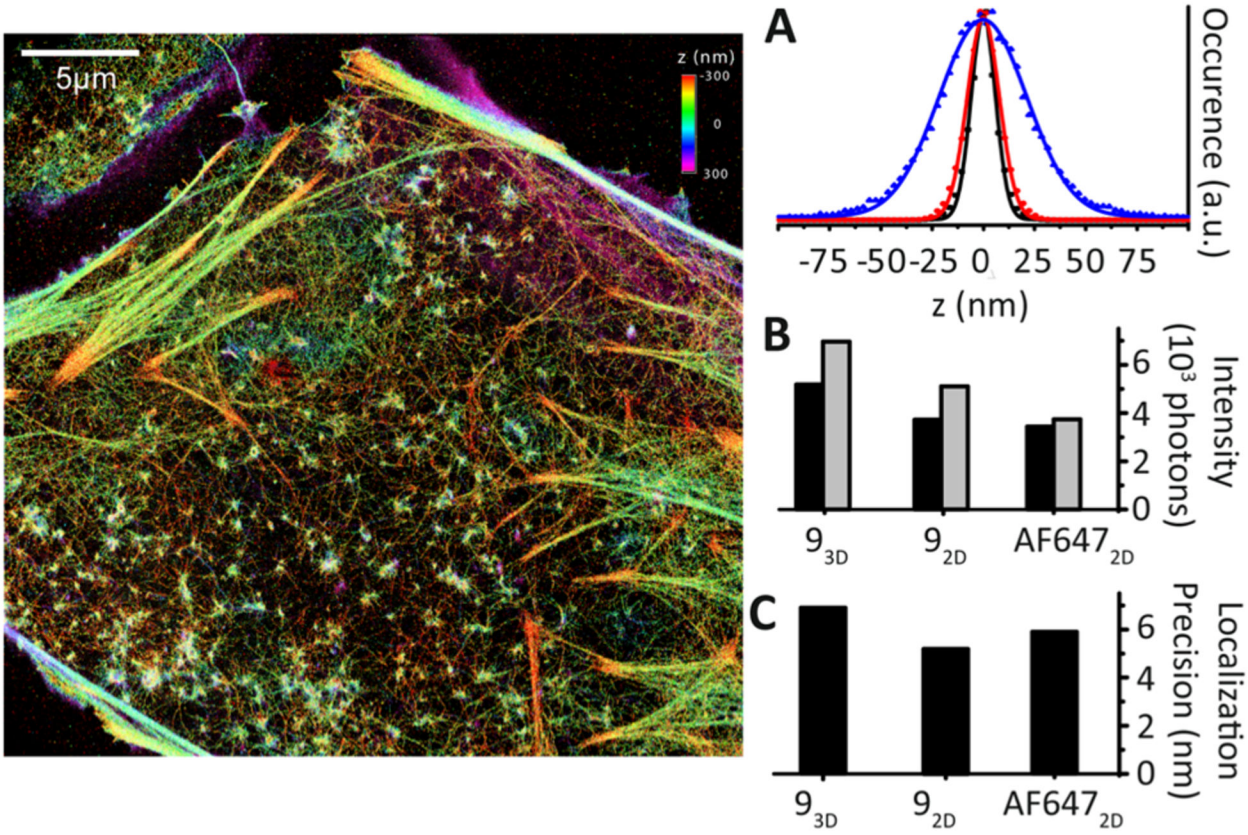

Figure 3.

Left: High quality 3D TRABI-BP SMLM image of F-Actin in a U2OS cell with **9**-phalloidin in PBS buffer. *Right*: (A) Lateral (x: black, y: red) and axial (blue) localization precisions calculated from the data illustrated on left. Marks indicate data points and solid lines indicate Gaussian fits to the data. (B) Comparison of single molecule photon intensities regarding single frame (black) and tracked (gray) median values of data illustrated in $\mathbf{9}_{3D}$ (left) and comparable measurements in 2D imaging modes of **9** (center) and AF647 (right) in standard *d*STORM photoswitching buffer. (C) Experimentally determined lateral localization precisions of $\mathbf{9}_{3D}$ (6.9 nm), $\mathbf{9}_{2D}$ (5.2 nm), and $AF647_{2D}$ (5.9 nm).

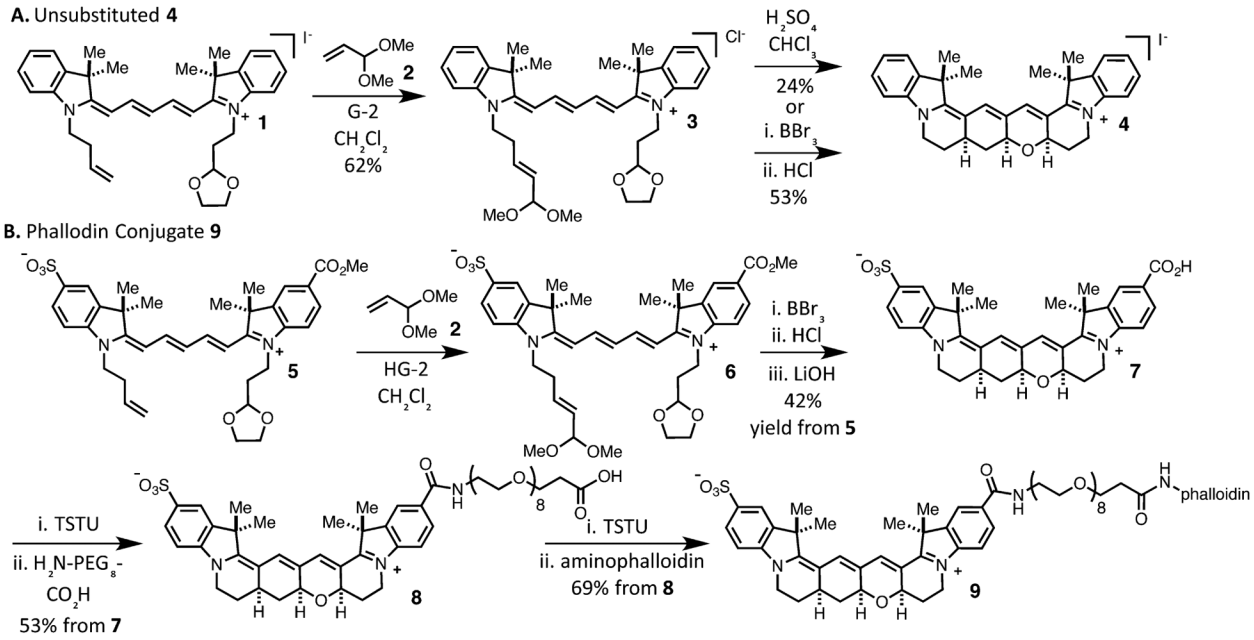

Scheme 1.
Synthetic Route to 4 (A) and 9 (B)